Development of an optical tweezer combined with micromanipulation for DNA and protein nanobioscience

G. V. Soni*,§, Feroz Meeran Hameed*,§, T. Roopa†,§ and G. V. Shivashankar*,†,#

*National Centre for Biological Sciences, Tata Institute of Fundamental Research, UAS-GKVK Campus, Bangalore 560 065, India
†Raman Research Institute, C. V. Raman Avenue, Bangalore 560 080, India

We have constructed an optical tweezer using two lasers (830 nm and 1064 nm) combined with micro-pipette manipulation having sub-pN force sensitivity. Sample position is controlled within nanometer accuracy using XYZ piezo-electric stage. The position of the bead in the trap is monitored using single particle laser backscattering technique. The instrument is automated to operate in constant force, constant velocity or constant position measurement. We present data on single DNA force-extension, dynamics of DNA integration on membranes and optically trapped bead–cell interactions. A quantitative analysis of single DNA and protein mechanics, assembly and dynamics opens up new possibilities in nanobioscience.

STUDY of single molecules and particles using micromanipulation methods presents a new paradigm in understanding the non-equilibrium behaviour of biological[1] and soft-matter physical systems[2]. It is now possible to manipulate individual DNA and protein molecules to explore a variety of novel phenomena that are screened in bulk studies[3]. Such studies have become possible due to the advent of experimental physical techniques such as optical tweezer[4], micropipette manipulation[5], scanning probe microscopy[6] (atomic force and near field optics) and single-molecule tracking methods[7]. The optical tweezer method allows one to probe forces to the limits of thermal noise. In this method, a laser beam is focused to a diffraction-limited spot to create a trap for the dielectric micron-sized Brownian particle[4]. The trapped particle is used as a molecular handle to study DNA elasticity[8], DNA–protein interactions[9], ligand–receptor interactions[10] and molecular motor dynamics[11], to name a few.

Individual DNA and protein molecules are good examples of flexible polymers. The bending and twisting of DNA polymers play an important role in defining the structures of DNA and are recognition motifs for DNA–protein interactions. Novel stress-induced structural transition has been explored using single-molecule manipulation of linear DNA at 70 pN force (B–S DNA transition) and in supercoiled DNA at 3 to 25 pN forces (B–P DNA transition)[3,8]. In comparison, the typical entropic forces are of the order of $K_B T/l_p < pN$, where l_p is the persistence length of DNA, K_B is the Boltzmann constant and T the temperature. On the other hand, the stalling forces exerted by RNA polymerase motors, which move on DNA, are in the range of 25 pN (ref. 9). The measurement of molecular forces opens up new avenues to understand structure–function relationship in biological systems at the level of single DNA and protein molecules. Such experiments demand further improvements in spatial and temporal force resolution.

In this article we describe the design, calibration and performance of a home-made optical tweezer with sub-pN force sensitivity. The construction is modular and allows us to combine a micropipette micromanipulation with the tweezer. In future, we plan to incorporate single-molecule detection methods with simultaneous operation of a dual optical tweezer and cross-correlation analysis of bead-position fluctuations. We present the experimental results on (a) DNA force extension experiment, (b) dynamics of DNA assembly on membrane tubules and (c) non-specific bead–T cell interaction force measurement using the optical tweezer set-up.
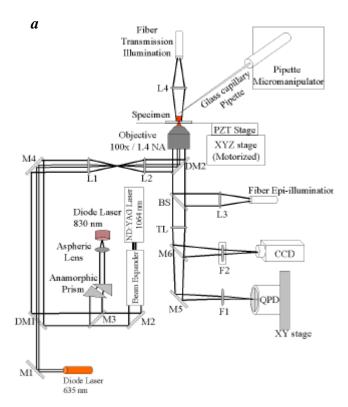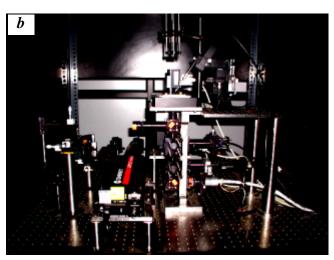
Instrument design

We have constructed two different versions of optical tweezers, one mounted on a home-made microscope (operating at two different wavelengths, 830 nm and 1064 nm) and the other (operating at 1064 nm) mounted on a commercial optical microscope (model IX 70, Olympus, Japan). Figure 1 a is a schematic of the experimental set-up constructed on the home-made microscope. To minimize noise due to vibrations, the instrument is built on a vibration isolation table (model 63-573; Technical Manufacturing Corporation, Peabody, MA, USA). The optical tweezer instrument is based on a custom-built microscope with a 100X objective (1.4 NA, oil immersion; Olympus). It incorporates three lasers, two lasers (1064 nm, ND : YAG, model 1064–200; Coherent,

---

Auburn, CA, USA, and 830 nm, GaAlAs diode, model 5430; SDL Inc., San Jose, CA, USA) which form the optical traps and one detection laser (635 nm, 5 mW power, model 31-0128; Coherent). The 1064 nm laser has a self-contained power supply, whereas the diode lasers are plugged into external power supplies. The 830 nm

a

b

Figure 1. *a*, Schematic of optical tweezer set-up. M1, M3, Near-IR dielectric mirrors. M2, M4, M5, M6, Silver-coated mirrors; DM1, DM2, Dichroic mirrors; L1, L2, Convex lens (f = 100 mm). L3, Convex lens (f = 50 mm); L4, Convex lens (f = 35 mm). TL, Tube lens (f = 200 mm). BS, 50/50 beamsplitter; F1, Filter (635/10); F2, Filter (450/100); *b*, Photograph of optical tweezer set-up mounted on the home-made microscope.

diode laser is powered by a variable voltage power supply with temperature controller support (model LDC-3724B; ILX Lightwave Corporation, Bozeman, Montana, USA), and the 635 nm diode laser by a 5V DC power supply (250 mA, model LDS1; Thorlabs, Newton, NJ, USA). The wavelengths of the trapping lasers were chosen to minimize heating of the sample and photodamage, since biological samples have minimal absorption in the near infrared wavelength[12]. The 0.9 mm diameter beam of the 1064 nm laser was expanded to 6.3 mm using a beam expander (model CWBX-6.0-7X-1064; CVI Laser Corporation, Albuquerque, NM, USA) to overfill the back focal plane of the objective lens which maximizes the trap stiffness. The 830 nm diode laser emits an uncollimated beam which is collimated using an aspheric lens (model C240TM; Thorlabs), and then circularized using an anamorphic prism (model AP-6X-10.0; CVI Laser Corporation). To enable manual steering of the laser beam, two convex lenses of equal focal lengths (Thorlabs) are mounted such that they are at a distance of 2*f* from each other, and also the second lens is at a distance of 2*f* from the back focal plane of the objective (see Figure 1 *a*). A dichroic mirror (model 775dcspxr; Chroma, Brattleboro, VT, USA) is used to reflect the lasers into the objective. The dichroic is chosen to give maximum reflectance of the trapping lasers into the objective and at the same time allowing transmission of the detection laser and visible light for imaging.

Precise motion of the sample with respect to the laser tweezer is achieved using a nanometer-precision three-axis piezo-electric transducer (PZT) stage (100 μm × 100 μm × 20 μm, model P-517.3CL; Physik Instrumente, Waldbronn, Germany) controlled by a LVPZT amplifier (model E-503.00; Physik Instrumente) with position servo controller (model E-509.C3; Physik Instrumente) and PZT displacement display (model E-515.03; Physik Instrumente). The position controller is interfaced to the computer through a shielded BNC connector board (model BNC-2090; National Instruments, Austin, TX, USA) connected to a 16-bit data acquisition board (PCI-MIO-16XE-10; National Instruments). Coarse movement of the sample is provided by a three-axis motorized stage consisting of three linear positioning stages (model M-126.DG; Physik Instrumente) controlled by a DC-motor controller (model C-844.40; Physik Instrumente) interfaced to the computer through a RS-232 interface.

Bright field illumination for imaging is achieved using a fibre optic microscope lamp (model PL-900; Dolan-Jenner, Lawrence, MA, USA), either in transmission or epi-illumination mode. In the epi-illumination mode, the beam from the fibre is reflected into the objective by a beamsplitter (model 21000; Chroma), mounted on a sliding holder below the dichroic. The light from the sample is collected by the objective, focused by a tube lens (Thorlabs) and reflected by a mirror (model 5102-NIR;

New Focus, San Jose, CA, USA) mounted on a sliding holder onto a CCD camera (model XC-77CE; Sony, Japan). An IR filter (model D450/100m; Chroma) on a filter slider helps to prevent damage to the CCD by the IR, and to visualize the IR beam when required for optical alignment. The image can be visualized on a TV monitor (model KV-B14PD1; Sony) and recorded on videotape through a video cassette recorder (model VC-MA33; Sharp, Japan) or digitized onto the computer using an image acquisition card (IMAQ card, model PCI-1411; National Instruments).

The bead position in the optical trap is monitored using the backscattering technique[13]. The backscattering of the 635 nm laser from the trapped bead is made to fall on a quadrant position detector (QPD; four element, segmented photodiode, model SPOT-4DMI; UDT sensors, Hawthorne, CA, USA) fitted on an XY stage (Thorlabs). The output currents from the four segments are fed into a Quadrant Amplifier (model 431 X-Y Position Indicator; UDT Instruments, Baltimore, MD, USA). The voltage output from the amplifier (a measure of the position of the trapped bead) is fed into the computer through the data acquisition board. The bandwidth of the detection system is 5 KHz limited by our current quadrant amplifier. The amplifier output voltages are also fed into an oscilloscope (model 54602B; Agilent Technologies, Palo Alto, CA, USA) for displaying the trapped bead displacement.

For micromanipulation, we use micropipettes pulled from borosilicate glass capillaries (BF120-94-10; Sutter Instrument Company, Novato, CA, USA) using a pipette puller (horizontal puller, model P-97; Sutter Instrument Company). The pulling is optimized to consistently give us micropipettes with tip size of about 1 μm and the taper length of a centimetre. The micropipette is coated with 3 nm of gold using a sputtering machine with a film thickness monitor (model sputter coater 108 auto; Pelco International; Redding, CA, USA). After coating, the micropipette is fixed onto a micromanipulator (left-handed motorized micromanipulator with remote, model DC3001; World Precision Instruments Inc., Sarasota, FL, USA). The micromanipulator allows the micropipette to be positioned relative to the trap and the detection laser in the sample plane. The trapped bead can be attached to the micropipette using the laser adsorption due to localized heating of the thin gold film[14]. The custom-made micropipettes, whose stiffness can be tuned by the fabrication process, offer a flexible alternative to atomic force cantilevers. In particular, these micropipette probes are useful in measuring larger forces (pN to nNs) not accessible with our current optical tweezer (fN to 10 pN). However, in this article we only present results pertaining to our optical tweezer to show the feasibility of sub-pN range force measurements. A photograph of the complete set-up is shown in Figure 1 b.

Calibration

The trapping lasers can be used to tweeze micron-sized beads. The two lasers provide traps of different stiffness ranges. The 1064 nm laser is used to form a relatively weak tweezer (with a maximum stiffness $\sim 1.7 \times 10^{-6}$ N/m for a 3 μm polystyrene particle at 200 mW laser power), and the 830 nm laser is used to form a strong tweezer (with a maximum stiffness of $\sim 2.8 \times 10^{-5}$ N/m for a 3 μm polystyrene particle at 150 mW laser power). The 635 nm detection laser is used to track the position of the bead in the optical trap.
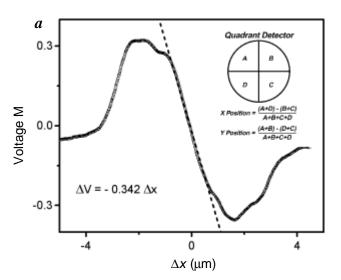
Quadrant calibration

Accurate position calibration of the QPD is required for precise measurement of the forces. A bead is stuck onto the glass cover slip, and the detection laser is incident on it. The backscattered light from the bead is then focused on the QPD. The response of the QPD with respect to the position of the bead (varied using the PZT stage) is used to calibrate the displacement to voltage characteristics of the QPD. The calibration is done on both the X and Y-axes and a typical (average of five trials) response characteristic of the QPD is plotted in Figure 2 a. The calibration curve is used to directly obtain the position of a bead in the trap from the measured QPD voltage. Since the solid angle of red laser illumination is same either on the fixed bead or on the trapped bead, the position calibration is consistent. The instrument is only used in the regime where the QPD shows linear response to the displacement of the trapped bead. Also the calibration is repeated for the different sizes of beads used in the experiments, as the response characteristics of each are different.
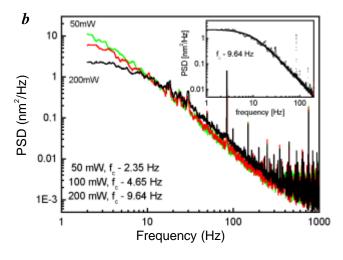
Trap stiffness calibration

The trap stiffness calibration[15] can be done using three different methods: (a) monitoring the variance in the bead position fluctuations, (b) the power spectrum analysis, and (c) by fitting the logarithm of the probability of the bead position fluctuations to a harmonic potential[13,16]. This is obtained by relating the potential $U = -K_B T \ln(P(x))$, where $P(x)$ is the position fluctuation histogram, K_B is the Boltzmann constant, and T is the temperature. Using equipartition theorem, the thermal fluctuation is related to the trap stiffness, $K_B T = K_{trap} \langle \Delta x^2 \rangle$, where $\langle \Delta x^2 \rangle$ is the variance of the position displacement of the bead in the optical trap. We use the K_{trap} deduced from the power spectrum analysis, which is not dependent on the QPD calibration and is also a more sensitive method. In Figure 2 b, we plot the power spectral density (PSD) of the position fluctuations of a particle in a trap at different laser power. The PSD is given by

$$\left\langle x(\boldsymbol{w})^2 \right\rangle = \frac{2\boldsymbol{g}K_{\mathrm{B}}T}{\boldsymbol{w}^2\boldsymbol{g}^2 + k^2} = \frac{K_{\mathrm{B}}T}{2\boldsymbol{g}\boldsymbol{p}^2[f^2 + f_{\mathrm{c}}^2]},$$

where f_c is the corner frequency and $\boldsymbol{g}$ is Stokes coefficient given by $\boldsymbol{g} = 6\boldsymbol{p}\boldsymbol{h}a$, a being the bead radius. The corner frequency of the power spectrum can be used to calculate the stiffness of the trap, $K_{\mathrm{trap}} = 12\boldsymbol{p}^2\boldsymbol{h}af_c$, where $\boldsymbol{h}$ is the viscosity of the medium, and $f_c = 9.64$ Hz (for 200 mW, 1064 nm laser power). Figure 2 b (inset) shows a typical Lorentzian fit to extract the corner frequency. From this method we estimate the trap stiffness to be $\sim 1.7 \times 10^{-6}$ N/m. Calibration of the tweezer is performed each time a measurement is made.

Results

We present three experiments to demonstrate the versatility of our instrument for single-molecule studies. In Figure 3, we plot the force extension curve of a single double-stranded *l*DNA molecule obtained using 830 nm laser trap with $K_{\mathrm{trap}} = 2.8 \times 10^{-5}$ N/m and 3 μm bead. The DNA molecule was anchored between a glass cover slip and a 3-micron sized polystyrene bead. The bead acts as a molecular handle to measure the entropic elasticity of DNA. Tethered beads are prepared by attaching one end of the *l*DNA (Cat.# SD0011; Fermentas, Hanover, MD, USA) to a cover slide and the other end to a 3 μm latex bead (Cat.# 17155-2; Polysciences Inc., Warrington, PA, USA) using a low-pH method[17,18]. Then, 5 μl (0.5 μg/μl) of *l*DNA, a 48.5 kb molecule, 16.5 μm in length, is first heated at 70°C for 5 min, and incubated together with 1 μl (10^6 beads/μl) of bead and 400 μl of PBS buffer (pH 6.0) for 20 min at room temperature. In this manner the bead–DNA link is obtained. A 12 mm diameter rubber 'o' ring glued with paraffin to a clean glass cover slip acts as the sample well. To link the other end of the DNA to the glass, 120 μl of the solution is pipetted into the sample well and incubated for 3 h at room temperature. After the biochemical attachment of DNA molecules to the beads, the sample cell is washed to flush out the untethered beads. The top is then covered with another cover slip to prevent evaporation of the buffer. The sample well is taped onto an aluminium sample holder, which is screwed onto the PZT stage for taking force extension curves. A DNA-tethered bead was trapped and moved in all four directions (in the *X–Y* plane) to check the uniformity in tether length ~ 16 μm, for the experiment. A
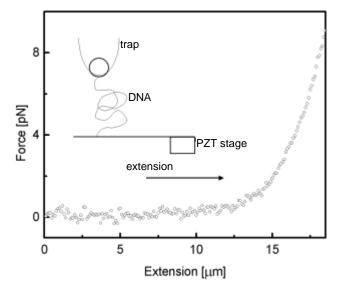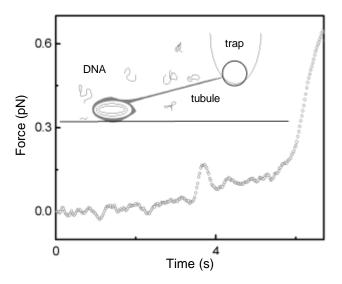

a

b

Figure 2. *a*, Quadrant calibration curve showing bead displacement to voltage characteristics along *X*-axis. The straight line fit to linear regime of the quadrant response is also shown. *b*, Power Spectral Density (PSD) of the trapped bead fluctuation at 50, 100 and 200 mW with the 1064 nm laser used for tweezing. Corner frequencies at these laser powers are 2.35, 4.65 and 9.64 Hz, which give a trapping stiffness of 0.4×10^{-6}, 0.8×10^{-6} and 1.7×10^{-6} N/m respectively. (Inset) Typical Lorentzian fit to the PSD (200 mW) to extract the corner frequency.

Figure 3. Double-stranded DNA force extension curve. A single DNA molecule was stretched using a trapped 3 μm bead attached to the end of the DNA and the force extension curves were recorded using 830 nm laser trap with $K_{\mathrm{trap}} = 2.8 \times 10^{-5}$ N/m.

cartoon of the experimental schematic is shown in Figure 3 (inset). The bead was held in the optical trap and the PZT stage was used to move the cover slip by precise steps of a few nanometres. The movement of the cover slip induces tension in the DNA. The position of the bead in the trap was recorded as a function of the movement of the PZT. The deflection of the bead from the centre of the trap can be used to calculate the force ($F = \Delta x K_{trap}$) on the DNA, and the movement of the PZT gives us the extension. The experiment was continued till the bead escaped from the trap. The data were taken using a fixed velocity of movement of the stage (~ 500 nm/s). The experiment was repeated and averaged over many curves to get the force extension curve shown in Figure 3, which clearly describes the entropic and elastic regimes of single-DNA elasticity. Typical entropic forces are of the order of $K_B T/l_p < $ pN, where $l_p = 50$ nm (ref. 19), and the elastic forces are in the regime of $K_B T$/base pair distance ~ 12 pN. DNA elasticity is well described by a worm-like chain model for polymers[20].

In Figure 4, using the tweezer mounted on the inverted microscope (IX70, Olympus), we plot the real-time dynamics of the integration of DNA molecules on cationic membrane vesicles, obtained using 1064 nm laser trap with $K_{trap} = 1.8 \times 10^{-6}$ N/m and a 2 μm bead. The DNA molecules, which are negatively charged, integrate on the membrane bilayer, with the cationic surfactant molecules acting as counter ions. Earlier studies in bulk have shown that DNA molecules form interesting structures with cationic lipids[21]. The DNA – membrane complexes are currently being investigated for non-viral gene delivery systems[22]. We have studied the dynamics of DNA assembly on the membrane tubule that has been drawn out of a vesicle using the optical trap. In our experiment, the vesicles that are made of didodecyl dimethyl ammonium bromide (DDAB) surfactant molecules are mostly multilamellar. A nonspecific electrostatic attachment was made between the optically-trapped bead and an isolated vesicle stuck to the glass cover slip mounted on the PZT stage. A membrane tubule of length 80–90 μm and radius < 100 nm was pulled out of the vesicle using a localized force exerted by the trapped bead. Change in the tubule length due to the integration of the oppositely charged DNA polymers on the membrane was observed by adding 2.5 μg of DNA (*l*DNA *Hin*dIII Digest, Cat# SM101-2; Fermentas, Hanover, MD, USA) to the sample cell. The lengths of the DNA molecules range from 125 bp (42.5 nm) to 23.13 kbp (7.8 μm). The DNA molecules integrate onto the membrane vesicles as a function of time due to charge interactions. Typical onset of DNA integration timescales are ~ 1 to 2 min depending on the local concentration. We observe changes in the length of the tubule as shown in Figure 4. The length of the tubule is found to decrease initially resulting in a small increase in force ~ 0.6 pN on the trapped bead due to DNA assembly. We are thus able to monitor the integration of the DNA molecules on the membrane bilayer using the optical tweezer and the tubule as a handle.

In Figure 5, we plot the force extension curves of non-specific bead–T cell interactions obtained using the 830 nm laser trap with $K_{trap} = 2.8 \times 10^{-5}$ N/m and 3 μm bead. The dynamics of the T cell receptor interaction kinetics have been extensively studied[23]. We measured the non-specific interaction of T cells with polystyrene beads. The cells were washed and then resuspended in mammalian Ringer's medium (160 mM sodium chloride, 4.5 mM potassium chloride, 1 mM magnesium chloride, 10 mM HEPES, and 11 mM glucose at pH 7.4) supplemented with 2 mM calcium chloride. Then the cells were transferred onto the 'o' ring sample well and allowed to stick to the cover slip at 37°C for 10 min. After incubation, the sample well was flushed with buffer to remove the floating cells and mounted on the optical tweezer set-up. Then 10^4 beads were added to 100 μl of sample volume. A bead was trapped and pushed against a cell. The deflection of the bead in the trap was used to calculate the interaction forces. The ascending part of the curve shows the force exerted by the tweezer on the cell membrane, and the retraction shows signatures of non-specific adhesion forces, if any. We vary the time of interaction between the bead and the cell membrane to measure non-specific interaction forces. The interaction time was controlled by varying the velocity of the PZT stage, 100 nm/s, 50 nm/s and 25 nm/s with typical interaction timescales ~ 5, 10 and 20 s respectively. As clearly seen in Figure 5, we observed that at 5 s interaction time, there was no evidence of non-specific adhesion, but as the timescale increased, a direct evidence of these interac-
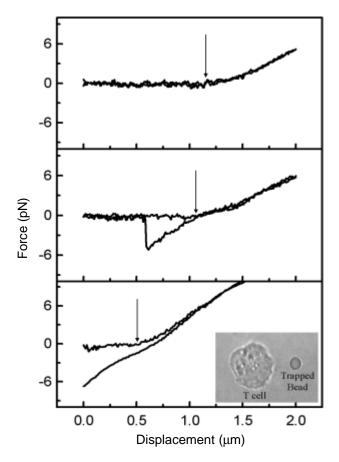

Figure 4. Typical force vs time plot to probe the dynamics of DNA integration on the membrane tubule measured using 1064 nm laser trap with $K_{trap} = 1.8 \times 10^{-6}$ N/m and a 2 μm bead. The force exerted on the trapped bead is a direct measure of the condensation of the tubule as a result of DNA assembly.

tions was observed. However for interaction timescales ~ 20 s, the rupture forces required to detach the bead from the cell membrane exceed that of the optical tweezer set-up. The non-specific interaction timescales and rupture forces are sensitive to the mode of preparation of the cells. From the data we can estimate the membrane tension of the T cells. Treating the trapped bead and the cell as springs in series, the effective spring constant is given by

$$\frac{1}{K_{\text{eff}}} = \frac{1}{K_{\text{trap}}} - \frac{1}{s}.$$

From the measured $K_{\text{eff}} = 47 \times 10^{-6}$ N/m and $K_{\text{trap}} = 28 \times 10^{-6}$ N/m, we estimate the membrane tension $s \sim 69 \times 10^{-6}$ N/m.

Figure 5. Non-specific interaction of polystyrene beads to T cells measured using the 830 nm laser trap with $K_{\text{trap}} = 2.8 \times 10^{-5}$ N/m and a 3 μm bead. The bead was held in the trap and pushed against the cell at different speeds to record the data. Plots show no interaction (***a***), a weak, non-specific interaction that ruptures on applying higher forces (> 6 pN) with the optical tweezer (***b***), and stronger non-specific interaction that cannot be ruptured with tweezer forces (***c***). Arrow shows the point of contact between the T cell and the bead. (Inset) Photograph of the trapped bead and a T cell in a typical experiment.

Conclusion

We have designed and built optical tweezers operating at two different wavelengths. The principal characteristics include (i) sub-pN force sensitivity, (ii) provision for dual trap and a wide range of trapping stiffness, (iii) noise reduction by optimizing the mechanical design and automation, and (iv) micropipette manipulation combined with optical tweezer for measurement of larger forces. The provision of a separate wavelength laser for position detection, which does not overlap with the trapping laser wavelengths, allows us to get an accurate position measurement which does not depend on the intensity of the trapping lasers. The PZT stage on which the sample holder is mounted gives us nanometre-scale precision. Computer control of the sample position maximizes the resolution of the sample holder movement in the X and Y-axes to ~ 3 nm, and in the Z-axis to < 1 nm. The quadrant calibration is done with the stuck bead being at the same solid angle of illumination as a bead in the optical trap to reduce errors. The vibration isolation table and a sturdy, mechanical design reduce the low frequency vibrations, which affect the tweezer efficiency and measurement resolution. The instrument can be programmed for velocity clamp, force clamp or position clamp. Typical measurement time resolution in our set-up is 0.2 ms, constrained by the quadrant amplifier bandwidth. In a recent experiment, we have used the set-up to track the correlated bacterial dynamics, where we have observed the mean forces ~ 76 fN exerted by the bacterial motion on the trapped bead[24].

1. Howard, J., *Mechanics of Motor Proteins and the Cytoskeleton*, Sinauer Associates Inc., 2001.
2. McCann, L. I., Dykman, M. and Golding, B., *Nature*, 1999, **402**, 785–787.
3. Strick, T., Allemand, J. F., Bensimon, D. and Croquette, V., *Annu. Rev. Biophys. Biomol. Struct.*, 2000, **29**, 523–543.
4. Ashkin, A., *Proc. Natl. Acad. Sci. USA*, 1997, **94**, 4853–4860.
5. Evans, E., Ritchie, K. and Merkel, R., *Biophys. J.*, 1995, **68**, 2580–2587.
6. Lewis, A., Radko, A., Ben Ami, N., Palanker, D. and Lieberman, K., *Trends Cell Biol.*, 1999, **9**, 70–73.
7. Peck, K., Stryer, L., Glazer, A. N. and Mathies, R. A., *Proc. Natl. Acad. Sci. USA*, 1989, **86**, 4087–4091.
8. Bustamante, C., Smith, S. B., Liphardt, J. and Smith, D., *Curr. Opin. Struct. Biol.*, 2000, **10**, 279–285.
9. Wang, M. D., Schnitzer, M. J., Yin, H., Landick, R., Gelles, J. and Block, S. M., *Science*, 1998, **282**, 902–907.
10. Evans, E., *Annu. Rev. Biophys. Biomol. Struct.*, 2001, **30**, 105–128.
11. Mehta, A. D., Rief, M., Spudich, J. A., Smith, D. A. and Simmons, R. M., *Science*, 1999, **283**, 1689–1695.
12. Neuman, K. C., Chadd, E. H., Liou, G. F., Bergman, K. and Block, S. M., *Biophys. J.*, 1999, **77**, 2856–2863.
13. Shivashankar, G. V., Stolovitzky, G. and Libchaber, A., *Appl. Phys. Lett.*, 1998, **73**, 291–293.
14. Shivashankar, G. V. and Libchaber, A., *ibid*, 1997, **71**, 3727–3729.

15. Gittes, F. and Schmidt, G. F. *Methods Cell Biol.*, 1998, **55**, 129–156.
16. Florin, E. L., Pralle, A., Stelzer, E. H. K. and Hörber, J. K. H., *Appl. Phys. A.*, 1998, **66**, S75.
17. Shivashankar, G. V., Feingold, M., Krichevsky, O. and Libchaber, A., *Proc. Natl. Acad. Sci. USA*, 1999, **96**, 7916–7921.
18. Allemand, J. F., Bensimon, D., Jullien, L., Bensimon, A. and Croquette, V., *Biophys. J.*, 1997, **73**, 2064–2070.
19. Bouchiat, C., Wang, M. D., Allemand, J. F., Strick, T., Block, S. M. and Croquette, V., *Biophys. J.*, 1999, **76**, 409–413.
20. Bustamante, C., Marko, J. F., Siggia, E. D. and Smith, S., *Science*, 1994, **265**, 1599–1600.
21. Koltover, I., Salditt, T., Radler, J. O. and Safinya, C. R., *ibid*, 1998, **281**, 78–81.
22. Chesnoy, S. and Huang, L., *Annu. Rev. Biophys. Biomol. Struct.*, 2000, **29**, 27–47.
23. Kim, S., Braunstein, N. S., Leonard, E. F. and Thomas J. L., *J. Immunol. Methods*, 2001, **249**, 73–84.
24. Soni, G. V., Jaffar Ali, B. M., Hatwalne, Y. and Shivashankar, G. V., *Biophys. J.* (in press).